

Needle-based refractive index measurement using low-coherence interferometry

Adam M. Zysk

Biophotonics Imaging Laboratory, Department of Electrical and Computer Engineering, Beckman Institute for Advanced Science and Technology, University of Illinois at Urbana-Champaign, 405 North Mathews Avenue, Urbana, Illinois 61801, USA

Steven G. Adie, Julian J. Armstrong, Matthew S. Leigh, Alexandre Paduch, and David D. Sampson

Optical+Biomedical Engineering Laboratory, School of Electrical, Electronic & Computer Engineering, University of Western Australia, 35 Stirling Highway, Crawley, Western Australia 6009, Australia

Freddy T. Nguyen and Stephen A. Boppart

Biophotonics Imaging Laboratory, Department of Electrical and Computer Engineering, Beckman Institute for Advanced Science and Technology, University of Illinois at Urbana-Champaign, 405 North Mathews Avenue, Urbana, Illinois 61801, USA

Received August 4, 2006; revised October 20, 2006; accepted November 3, 2006;
posted November 7, 2006 (Doc. ID 73819); published January 26, 2007

We present a novel needle-based device for the measurement of refractive index and scattering using low-coherence interferometry. Coupled to the sample arm of an optical coherence tomography system, the device detects the scattering response of, and optical path length through, a sample residing in a fixed-width channel. We report use of the device to make near-infrared measurements of tissues and materials with known optical properties. The device could be used to exploit the refractive index variations of tissue for medical and biological diagnostics accessible by needle insertion. © 2007 Optical Society of America
OCIS codes: 170.4500, 110.2350, 290.3030.

Optical contrast is increasingly being exploited in the localization and evaluation of diseased tissue. Interferometric detection techniques such as low-coherence interferometry (LCI) and optical coherence tomography (OCT) have been used in medicine and biology to visualize structural features. These techniques use broadband near-infrared light to noninvasively penetrate up to several millimeters into dense tissue and provide real time depthwise mapping of backscattered light with spatial resolution approaching that of light microscopy.

LCI and OCT perform sensitive measurements of axial optical path length (OPL), a fact that has been exploited to measure refractive indices in bulk tissues.^{1–3} Techniques using modified OCT systems have been developed to image the refractive index (RI). Projected index computed tomography computationally reconstructs the RI by measuring the displacement of a known reference within the sample at multiple angular and lateral positions.⁴ Bifocal optical coherence refractometry maps the RI of a sample by scanning a pair of foci along the sample depth and measuring the OPL between them.⁵ Though these interferometric RI measurement and imaging techniques may be suited for *in vivo* imaging, their penetration depth is limited to that of OCT and LCI. To apply OCT and LCI to tissues deep within a patient, interferometric forward sensing devices have been developed for use in conjunction with catheters, endoscopes, and needles.^{6–8} To our knowledge, however, no forward sensing device has demonstrated RI measurement capabilities.

The RI variations present within tissue are known to hold diagnostic significance. Among subcellular

structures, for instance, the RI varies by up to $\Delta n \approx 0.11$.^{9,10} These variations may potentially yield indicators of disease state, since morphological changes occur in these structures during the progression of many diseases. One potential application is breast tumor detection. Recent research indicates that significant RI variations exist between the adipose tissue comprising the majority of the breast and cancerous or epithelial structures of diagnostic interest.¹¹ Therefore RI measurement may be a means of rejecting fat tissue, thereby reducing the high nondiagnostic sampling rate¹² of routine needle biopsy procedures.

We have constructed a prototype needle-based device for the measurement of RI and depth-resolved

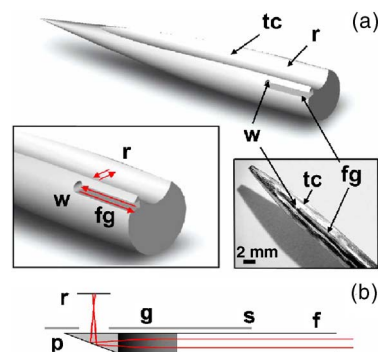


Fig. 1. Needle-based refractive index measurement probe. (a) Illustrations of the needle housing design and photograph of the prototype. (b) OCT-coupled optical fiber probe showing the beam path geometry. fg, fiber groove; f, ferrule; s, metal sleeve; g, GRIN lens; p, right-angle prism; w, window; tc, tissue channel; r, reflective surface.

scattering (Fig. 1). It is designed to direct tissue into a narrow channel (tc, 0.98 mm wide) as the needle (4.7 mm diameter) is inserted. Light from the sample arm of an OCT system is transmitted through the tissue channel and backreflected from a reflective surface (r). In this implementation, light is introduced via a single-mode fiber (SMF-28) probe located in a groove (fg) along the side of the needle. The micro-optics attached to the end of the fiber are similar to those used in side-imaging endoscopic OCT devices.¹³ They consist of a ferrule and gradient index (GRIN) lens (DiCon Fiberoptics, Richmond, California) cemented to the polished fiber end, weakly focusing (working distance=4.4 mm, NA=0.02) across the channel. The optical cement (Norland Products, Cranbury, New Jersey) window provides a seal between the tissue channel and fiber groove. The fiber and micro-optics are fastened and sealed in the groove with layers of epoxy and silicone to ensure a watertight seal. The probe was connected to a spectral-domain OCT system employing a superluminescent diode source ($\lambda_0=1310$ nm, $\Delta\lambda=91$ nm, B&W Tek, Newark, Delaware), an optical circulator with a 5:95 splitter (Gould Technology, Millersville, Maryland), and a line scan camera (SU1024LE, Sensors Unlimited, Princeton, New Jersey) capable of acquiring 10,000 scan lines/s with a signal-to-noise ratio of 105 dB while exposing the sample to ~ 6 mW of incident power.

The axial position of an object in an OCT image is dependent upon the OPL. For normal incidence, the OPL to a reflector positioned behind a heterogeneous sample is related to the group RI, $n_g(z)$, of the sample along the optical beam path by

$$\text{OPL}_{\perp} = \int_0^l n_g(z) dz, \quad (1)$$

where l is the physical reflector position and z is the direction of propagation. When the physical reflector position is known, the mean group RI of a sample is given by

$$\bar{n}_g = \frac{\text{OPL}_{\perp}}{l}. \quad (2)$$

Deviations from normal incidence at the window-tissue interface may result in refraction and an RI-dependent lateral shift of incident position at the tissue-reflector interface. The ratio of the normal OPL (OPL_{\perp}) to the refracted OPL (OPL_{ref}) is given by

$$\frac{\text{OPL}_{\perp}}{\text{OPL}_{\text{ref}}} = \cos \left[\theta_1 - \sin^{-1} \left(\frac{n_1 \sin \theta_1}{n_2} \right) \right] - \sin \left[\theta_1 - \sin^{-1} \left(\frac{n_1 \sin \theta_1}{n_2} \right) \right] \tan \theta_2, \quad (3)$$

where n_1 and n_2 are the phase RIs of the optical window and tissue, respectively, and θ_1 and θ_2 are the respective (clockwise) deviations of the window-tissue and tissue-reflector interfaces from normal incidence. These tilts produce a nonlinear response in

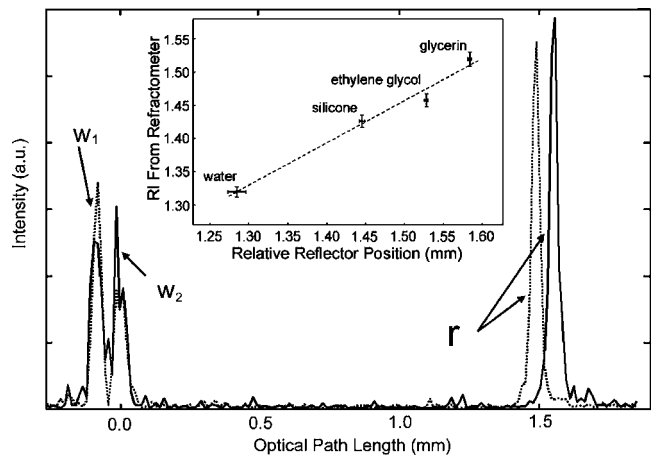


Fig. 2. Average of 400 axial scans of silicone fluid and glycerin. Axial position of the reflector (r) depends on the refractive index of the sample contained between the sample-window interface (w_2) and r . Thin silicone layer w_1 - w_2 is also visible. Inset: calibration of relative reflector position to refractometer measurements.

the OPL_{ref} versus RI curve that may yield inaccurate results if data are analyzed based on Eq. (2). However for interface angles below 10° , the linearity of the needle response is within 0.5% when $1.3 < n_2 < 1.6$.

Since the exact beam geometry is difficult to measure in this device, calibration spanning the range of tissue RIs was undertaken with clear solutions of water, silicone fluid, ethylene glycol, and glycerin. A transmission refractometer¹⁴ at 1310 nm was used to measure the displacement of a collimated beam through each liquid at a single incident angle. Determined from air and water [$n=1.322$ at 1310 nm (Ref. 15)] measurements, the incident angle was used to find RI via Snell's Law. The needle calibration is shown in Fig. 2. The RI error bars are due to beam position and sample width measurement uncertainties and the reflector position error bars indicate the standard deviation. Differences between phase and group RI may contribute a small deviation, which is not included here. A linear fit to the data yielded a good match ($r^2=0.98$), enabling measurement of samples within the calibrated range.

To demonstrate measurement of scattering samples, Intralipid and fresh chicken muscle, liver, skin, and fat tissues were analyzed. Representative axial scans from several samples are shown in Fig. 3. The axial positions of the window-tissue and tissue-reflector interface reflections were found by determining the optimal Gaussian fit to the boundary responses in each axial scan. Note that alternatively w_1 could be utilized for calibration and analysis if w_2 cannot accurately be detected, e.g., due to strong sample scattering. The RI of the sample was found by measuring the channel OPL and applying the linear fit from calibration. Table 1 shows the average RI values calculated from 400 total axial scans recorded at two locations in each sample. These values are consistent with previously reported values for various animal and human tissues.^{15,16} The relatively higher standard deviations in skin and fat are likely due to

sample heterogeneity. Multipatient studies are necessary to verify the full utility of *in vivo* human tissue RI measurements.

Future work includes miniaturizing this device for *in vivo* use. Core needle biopsy devices have a diameter of approximately 0.9 mm (e.g., Easy Core 20G, Boston Scientific, Natick, Massachusetts), which requires a significant decrease in the tissue channel size. A trade-off exists between the channel width l and RI resolution Δn given by $\Delta n = n / (1 + l/l_c)$, where l_c is the source coherence length. A miniaturized probe with a channel width of 0.6 mm would have $\Delta n = 0.019$ when the source from this experiment is used to measure tissue with $n = 1.4$; a source with $l_c = 3.0 \mu\text{m}$ would yield $\Delta n = 0.007$. Such miniaturization of the needle housing may require microfabrication techniques, and the dimensions involved are within current capabilities. Custom manufacturing and alignment may also be required for the optical components. In particular, the GRIN lens and microprism are not widely available at appropriate sizes but could be replaced by multimode optical fiber¹⁷ and a right-angled reflective element.

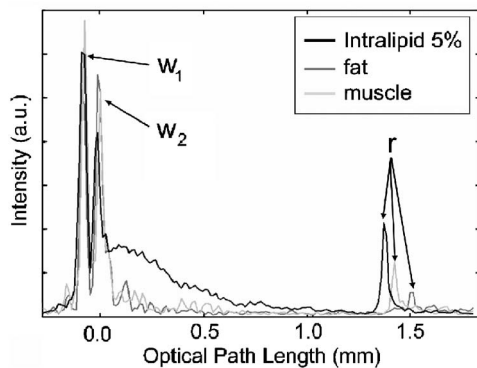


Fig. 3. Averaged axial scan responses of Intralipid and chicken tissue. Scattering from the sample is visible between w_2 and r . w_1 , window layers interface; w_2 , tissue-window interface; r , tissue-reflector interface.

Table 1. Refractive Index Values of Intralipid and Chicken Tissue Measured with the Prototype Needle Device^a

| Sample | Refractive Index | |
|----------------|-------------------------------|--------------------------------------|
| | Mean \pm Standard Deviation | Previously Reported Refractive Index |
| Intralipid 5% | 1.333 \pm 0.024 | 1.33 (Ref. 15) |
| Intralipid 10% | 1.351 \pm 0.009 | 1.34 (Ref. 15) |
| Muscle | 1.399 \pm 0.013 | 1.40-1.41 (Ref. 16) |
| Liver | 1.410 \pm 0.014 | 1.37-1.39 (Ref. 16) |
| Skin | 1.424 \pm 0.022 | 1.37-1.42 (Ref. 15) |
| Fat | 1.450 \pm 0.014 | 1.46 (Ref. 16) |

^aThe values are compared with published values of Intralipid (1310 nm) and human, canine, porcine, and bovine tissue (633–1310 nm).

In conclusion, we have demonstrated a needle-based technique for measuring RI and scattering and tested it with scattering phantoms and tissues. Although the prototype is larger than desirable for use *in vivo*, we have demonstrated the feasibility of this needle design. Its measurement capabilities may be useful in a variety of biological and clinical applications.

We thank Julia Hoyer for assistance with device fabrication and Sergey Alexandrov for providing useful discussion. Research conducted by S. A. Boppart at the University of Illinois at Urbana-Champaign was supported by the UIUC-UIC Intercampus Research Initiative in Biotechnology and the National Science Foundation (grant BES 03-47747). A. M. Zysk received travel and fellowship support from the National Science Foundation East Asia and Pacific Summer Institutes for U.S. Graduate Students (grant 0413596) in collaboration with the Australian Academy of Science. S. A. Boppart's e-mail address is boppart@uiuc.edu.

References

1. S. A. Alexandrov, A. V. Zvyagin, K. K. M. B. D. Silva, and D. D. Sampson, *Opt. Lett.* **28**, 117 (2003).
2. W. V. Sorin and D. F. Gray, *IEEE Photon. Technol. Lett.* **4**, 105 (1992).
3. G. J. Tearney, M. E. Brezinski, J. F. Southern, B. E. Bouma, M. R. Hee, and J. G. Fujimoto, *Opt. Lett.* **20**, 2258 (1995).
4. A. M. Zysk, J. J. Reynolds, D. L. Marks, P. S. Carney, and S. A. Boppart, *Opt. Lett.* **28**, 701 (2003).
5. A. V. Zvyagin, K. K. M. B. D. Silva, S. A. Alexandrov, T. R. Hillman, J. J. Armstrong, T. Tsuzuki, and D. D. Sampson, *Opt. Express* **11**, 3503 (2003).
6. S. A. Boppart, B. E. Bouma, C. Pitris, G. J. Tearney, J. G. Fujimoto, and M. E. Brezinski, *Opt. Lett.* **22**, 1618 (1997).
7. X. Li, C. Chudoba, T. Ko, C. Pitris, and J. G. Fujimoto, *Opt. Lett.* **25**, 1520 (2000).
8. X. Liu, M. J. Cobb, Y. Chen, M. B. Kimmey, and X. Li, *Opt. Lett.* **29**, 1763 (2004).
9. J. Beuthan, O. Minet, J. Helfmann, M. Herrig, and G. Muller, *Phys. Med. Biol.* **41**, 369 (1996).
10. A. Dunn and R. Richards-Kortum, *IEEE J. Sel. Top. Quantum Electron.* **2**, 898 (1996).
11. A. M. Zysk, E. J. Chaney, and S. A. Boppart, *Phys. Med. Biol.* **51**, 2165 (2006).
12. R. M. Pijnappel, M. van den Donk, R. Holland, W. P. T. M. Mali, J. L. Peterse, J. H. C. L. Hendriks, and P. H. M. Peeters, *Br. J. Cancer* **90**, 595 (2004).
13. J. J. Armstrong, M. S. Leigh, D. D. Sampson, J. H. Walsh, D. R. Hillman, and P. R. Eastwood, *Am. J. Respir. Crit. Care Med.* **173**, 226 (2006).
14. S. Nemoto, *Appl. Opt.* **31**, 6690 (1992).
15. H. Ding, J. Q. Lu, K. M. Jacobs, and X. H. Hu, *J. Opt. Soc. Am. A* **22**, 1151 (2005).
16. F. P. Bolin, L. E. Preuss, R. C. Taylor, and R. J. Ference, *Appl. Opt.* **28**, 2297 (1989).
17. W. A. Reed, M. F. Yan, and M. J. Schnitzer, *Opt. Lett.* **27**, 1794 (2002).